ELSEVIER

Materials Science and Engineering A314 (2001) 140–149

MATERIALS SCIENCE & ENGINEERING A

www.elsevier.com/locate/msea

# Influence of mercury environment on the fatigue behavior of spallation neutron source (SNS) target container materials

H. Tian [a,*], P.K. Liaw [a], H. Wang [b], D. Fielden [a], J.P. Strizak [b], L.K. Mansur [b], J.R. DiStefano [b]

[a] *Department of Materials Science and Engineering, The University of Tennessee, Knoxville, TN 37996-2200, USA*
[b] *Oak Ridge National Laboratory, Oak Ridge, TN 37831, USA*

**Abstract**

The high-cycle fatigue behavior of 316 LN stainless steel (SS), the prime candidate target-container material for the spallation neutron source (SNS), was investigated in air and mercury at frequencies from 10 to 700 Hz with a $R$ ratio of 0.1. A decrease in the fatigue life of 316 LN SS in air was observed with increasing frequency. However, little influence of frequency on fatigue life was found in mercury. An increase in the specimen temperature at 700 Hz seems to be the main factor that contributed to the decrease of the fatigue life in air, relative to that at 10 Hz. However, because of the cooling effect of mercury, only a small temperature increase was found at 700 Hz, and, therefore, there was little frequency influence in mercury. At 10 Hz, a shorter fatigue life of 316 LN SS was measured in mercury than in air at stresses greater than yield strength, which may have resulted from liquid metal embrittlement (LME). At lower stresses, no difference in fatigue lives between mercury and air was detected at 10 Hz. At 700 Hz, the fatigue life in mercury was longer than in air. The fatigue endurance limit measured at both frequencies in mercury and in air was approx. 350 MPa. © 2001 Elsevier Science B.V. All rights reserved.

*Keywords:* Spallation neutron source; Mercury environment; Fatigue behavior

## 1. Introduction

Type 316 stainless steel (SS) has been widely used in the nuclear industry, because of its excellent ductility, corrosion resistance, and irradiation performance. Recently, 316 LN (low carbon, nitrogen-containing) SS was selected as a container material for the mercury target of the Spallation Neutron Source (SNS) at the Oak Ridge National Laboratory (ORNL) [1].

The target material for the bombardment of a proton beam will be liquid mercury (Hg) contained in the 316 LN SS container. The function of the neutron-source system is to convert a short-pulsed, high-power high-energy proton beam into a short-pulsed, low-energy neutron beam optimized for use in neutron-scattering instruments [2]. The container will be subjected to irradiation by both protons and neutrons, as well as to cyclic pressure waves produced by pulse-induced rapid heating of the contained mercury. Therefore, an investigation of the effect of mercury on the fatigue behavior of 316 LN SS is necessary to assure the integrity of target-container materials. In particular, it is desirable to assess whether the phenomenon of liquid metal embrittlement (LME) can occur and affect mechanical behavior of the alloy in contact with mercury.

The phenomenon of LME was first reported in 1874, but a comprehensive text on the subject was not published until 1960 [3]. Investigation of LME has been carried out on various aluminum alloys, nickel alloys, Monel alloys, and highly-stressed mild steels [4–9], but there is less information available for stainless steels. In the past, LME was studied mainly by means of uniaxial tension tests or slow-strain-rate tension tests, rather than cyclic loading tests [4–7]. Several materials tested in mercury were found to exhibit more brittle fracture characteristics than in air [5–7]. Some research results showed similar fracture characteristics of nickel-based alloys in gaseous hydrogen and liquid mercury, while other results reported that the fracture modes were distinguishable in these two conditions, with more intergranular cracking in mercury than hydrogen [5–7]. LME was found to be more severe in nickel and copper

* Corresponding author..

0921-5093/01/$ - see front matter © 2001 Elsevier Science B.V. All rights reserved.
PII: S0921-5093(00)01919-5

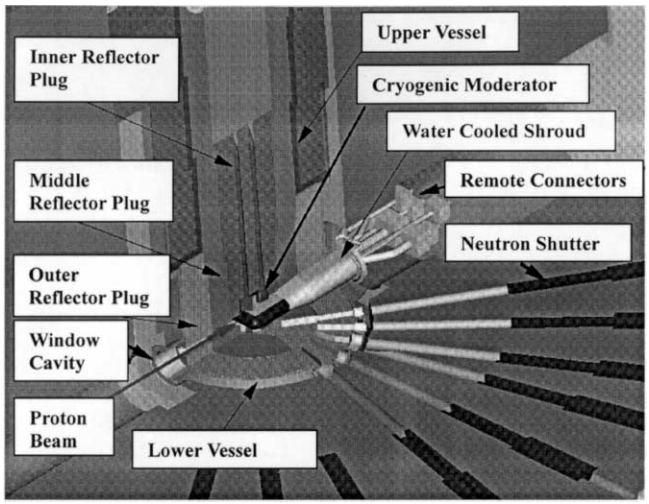


Fig. 1. Cutaway view of the target facility of the spallation neutron source [13]. The mercury target is shown intercepting the proton beam. The neutron beam tubes are presented in the lower right quadrant. Neutron moderators and neutron reflectors are labeled, as are several other structural and auxiliary components.

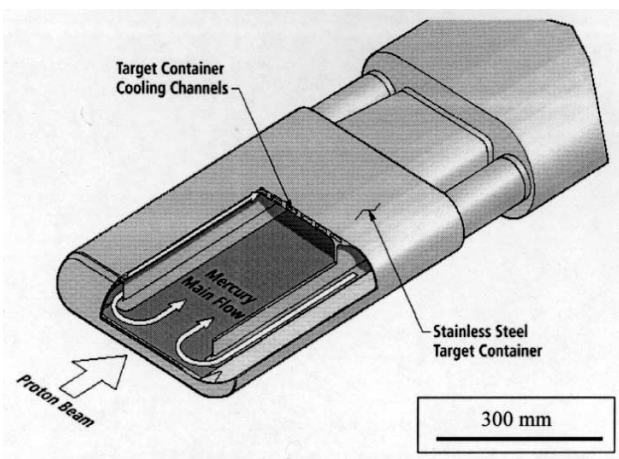


Fig. 2. Illustration of the target container of the spallation neutron source [13].

alloys than in steels because of the limitation of wetting between the mercury and steel [7].

The present studies focused on the fatigue behavior of 316 LN SS in air and mercury within the test frequency range from 10 to 700 Hz using an advanced high-frequency electrohydraulic machine.

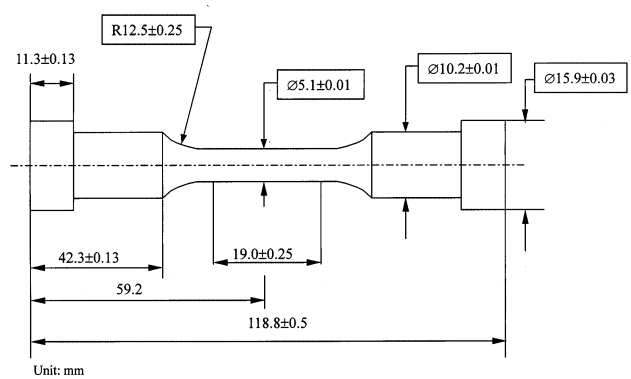


Fig. 3. Dimension of fatigue specimen of 316 LN stainless steel. The specimens are fabricated utilizing low-stress grinding.

## 2. Spallation neutron source (SNS)

The SNS is an accelerator-based instrument that provides pulsed beams of neutrons by bombarding a mercury target with 1 GeV protons [2,10–13]. The facility is being designed to fulfill the needs of the neutron-scattering community well into the next century. The Department of Energy (DOE) plans to invest more than 1.3 billion dollars in design and construction of the SNS facility. In the broadest terms, the facility consists of an ion source, a linear accelerator, a proton storage ring, and a target station. The target station includes the mercury target, neutron moderators, neutron beam tubes and neutron scattering instruments. The target is positioned within an iron and concrete shielding monolith approx. 12 m in diameter. Fig. 1 shows a cutaway view of the target and beam-tube region.

A heavy liquid-metal target was selected over a water-cooled solid target for many reasons. These include higher neutron production, increased power-handling capability, and the absence of radiation damage to the liquid target. However, the target container material will experience radiation damage. The performance of the target container material to the intended service is crucial to the successful operation of the SNS facility. The configuration of the target container of the SNS is shown in Fig. 2. The container is a four-walled structure. The outer two walls define a protective shroud cooled by water in an enclosed channel, and the inner two walls form a mercury channel. The mercury serving as the target material is contained by the innermost wall.

Table 1
Chemical composition of type 316 LN stainless steel in weight percent (wt.%) [14]

| Element | C | Mn | P | S | Si | Ni | Cr | Mo | Co | Cu | N | Fe |
|---|---|---|---|---|---|---|---|---|---|---|---|---|
| wt.% | 0.009 | 1.75 | 0.029 | 0.002 | 0.39 | 10.2 | 16.31 | 2.07 | 0.16 | 0.23 | 0.11 | Bal. |

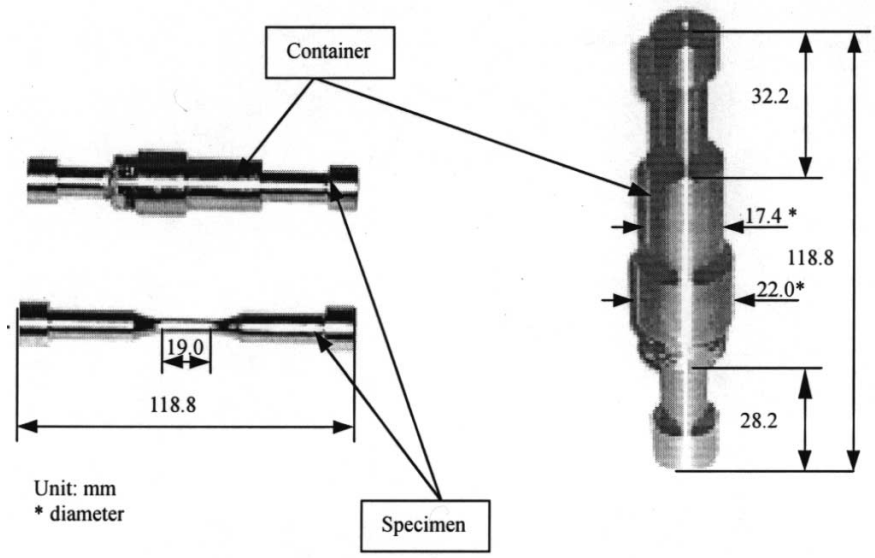


Fig. 4. Specially-designed specimen for fatigue testing in mercury.

Fatigue tests and analyses of the 316 LN SS container material, in addition to a comprehensive battery of other tests and calculations [13], are deemed necessary to qualify the material for service. The interaction of the energetic proton beam with the mercury target leads to high heating rates in the target. Although the resulting temperature rise is only a few °C per beam pulse, the associated expansion of the mercury leads to the production of pressure waves that interact with the container walls.

Research results on the fatigue properties of 316 LN SS have been reported in the literature [15,16]. There are some other studies that have been carried out on the fatigue behavior of 316 LN SS in environments such as hydrogen, sodium, and chloride [17–19]. However, little work has been done concerning the fatigue behavior of 316 LN SS in a mercury environment. Recent tensile test results, comparing behavior in mercury and air, have shown negligible differences, i.e. mercury did not affect the mechanical behavior of type 316 SS [13,20].

## 3. Experimental procedures

Type 316 LN SS is an austenitic stainless steel with the chemical composition shown in Table 1. The geometry of the cylindrical-bar specimen used is illustrated in Fig. 3. The specimen has a total length of 118.8 mm, a gage length of 19.0 mm, and a diameter of 5.1 mm. In order to conduct fatigue tests in a mercury environment, an attached container of 304 stainless steel was used (Fig. 4). The gage section of the specimen was immersed in mercury enclosed in the container. The container was attached to the specimen with a silicone-rubber adhesive sealant, which could be removed from the specimen after the test, and reused. During fatigue tests, the gage section of the specimen remained in contact with the mercury in the container.

Two state-of-the-art electrohydraulic material test system (MTS) were used in the present study. One has a frequency range from 0.001 to 60 Hz and is capable of being operated in a vacuum as low as $10^{-6}$ torr. It can be used to run tests at temperatures as high as 2000°C in either vacuum or inert gas. The second machine is an advanced, high-frequency, electrohydraulic MTS machine with a frequency range from 20 to 1000 Hz and a loading capacity of $\pm 25$ kN. Servovalves are activated by voice coils to achieve frequencies up to 1000 Hz. To avoid testing noise at 1000 Hz, the machine is situated in a well-designed, soundproof room equipped with a heat pump, which has the cooling capability to prevent overheating of the servovalves.

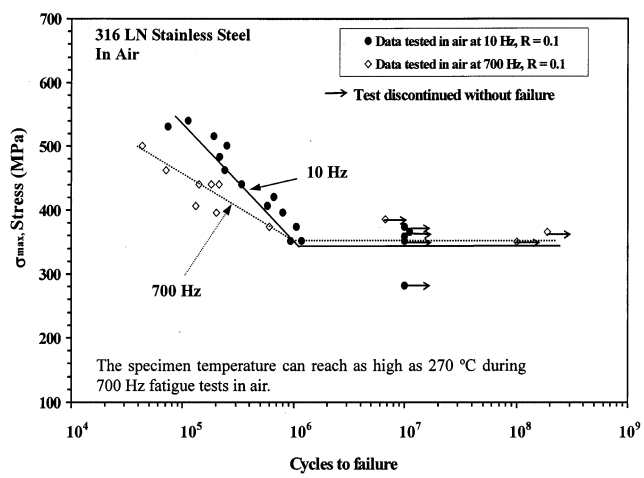


Fig. 5. Effect of test frequency on the fatigue life of 316 LN SS in air.

Table 2
Tensile properties of 316 LN stainless steel [14]

| Temperature (°C) | Strain rate (1 $s^{-1}$) | Apparent modulus (1000 MPa) | 0.2% Yield strength (MPa) | Tensile strength (MPa) | Elongation (%) | Reduction of area (%) |
|---|---|---|---|---|---|---|
| 21 | 0.01 | 186 | 288.0 | 587.2 | 60.0 | 82.6 |

In the mercury-environment fatigue test, an airflow system (Model MINI-PAC) was used to filter the air near the specimen to eliminate the possibility of mercury entering the room. Following the fatigue tests in mercury, the specimens were washed in acetone with an ultrasonic cleaning machine (Model FS20) for 1 h.

High-cycle fatigue (HCF) tests at different stress levels were conducted in air and mercury under a load-control mode using a $R$ ratio of 0.1, where $R = \sigma_{min}/\sigma_{max}$, $\sigma_{min}$ and $\sigma_{max}$ are the applied minimum and maximum stresses, respectively. High-frequency tests in the frequency range of 10 to 700 Hz were performed using the 1000 Hz machine to study the frequency effect on fatigue behavior. To assure the reliability and repeatability of the fatigue test results in mercury, some fatigue experiments conducted at the University of Tennessee, Knoxville (UTK) were compared with the ongoing test program at the Oak Ridge National Laboratory (ORNL). The experimental details in the mercury-environment fatigue tests at ORNL were similar to those described above.

A high-speed and high-sensitivity, thermography-infrared (IR) detection method was used to observe changes in the specimen temperature during fatigue. This technique uses IR radiation emitted from the surface of a material to determine its temperature. The equipment employed in the experiment is a state-of-the-art, high-resolution, Raytheon-Radiance-HS IR imaging system — an IR camera, which has a temperature resolution up to $10^{-2}$°C and a spatial resolution of 5.4 μm. Under the snapshot mode, the IR camera has a tunable data-acquisition speed up to 6,100 Hz, and was used to measure the specimen temperature during fatigue testing. A thin sub-micron graphite coating was applied on the specimen gage-length section of the as-machined sample to decrease the surface-heat reflection. Following fatigue tests, a scanning-electron microscope (SEM), Model Cambridge S-360, was used to observe the fracture surfaces.

## 4. Results and discussion

### 4.1. Basic S (applied stress) – N (cycles to failure) curve

Fatigue experiments were conducted at different stress levels. Test results in air are illustrated in Fig. 5. In this test series, efforts were mainly focused on tension–tension fatigue tests with a $R$ ratio of 0.1. Table 2 shows that the yield-strength of 316 LN SS is approx. 288 MPa and ultimate tensile strength is about 587 MPa at a strain rate of 0.01 $s^{-1}$. The maximum stresses used in the present fatigue tests were between approx. 270 and 540 MPa (Fig. 5).

In Fig. 5, the 316 LN SS exhibits a fatigue endurance limit of about 350 MPa at 10 Hz ($R = 0.1$), and fatigue tests conducted at 700 Hz also showed a similar limit. At the stress level near 350 MPa, the fatigue data exhibit some scatter. This is probably due to an in-

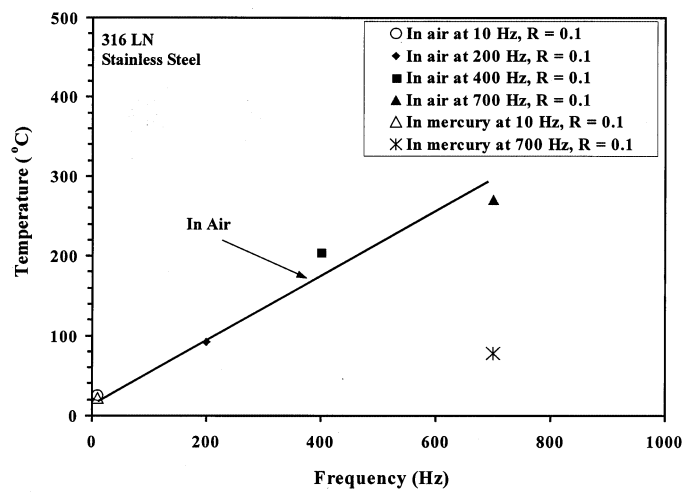


Fig. 6. Variation of specimen temperature with test frequency during fatigue tests of 316 LN SS in air and mercury at $\sigma_{max} = 439$ MPa.

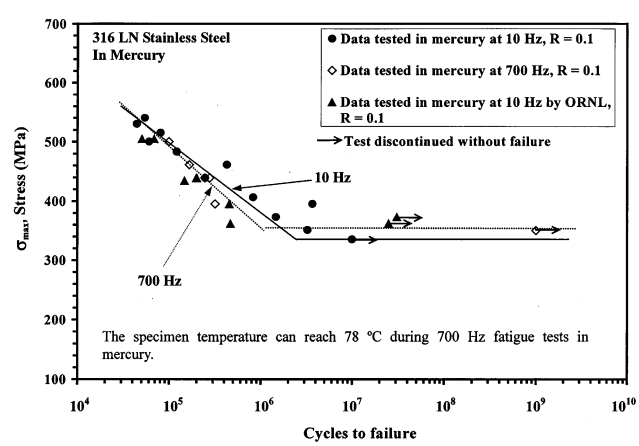


Fig. 7. Effect of test frequency on the fatigue life of 316 LN SS in mercury.

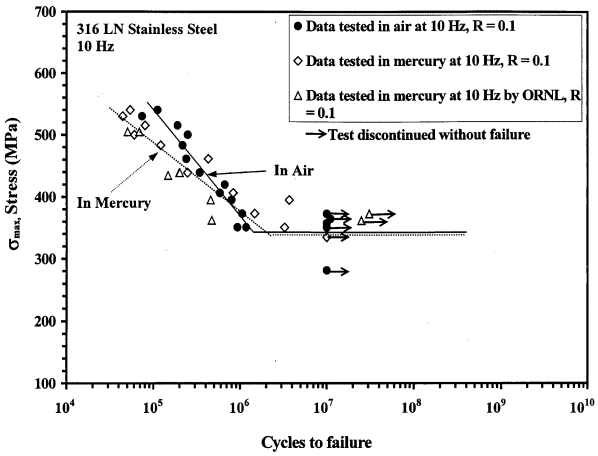


Fig. 8. Effect of mercury environment on the fatigue life of 316 LN SS at 10 Hz.

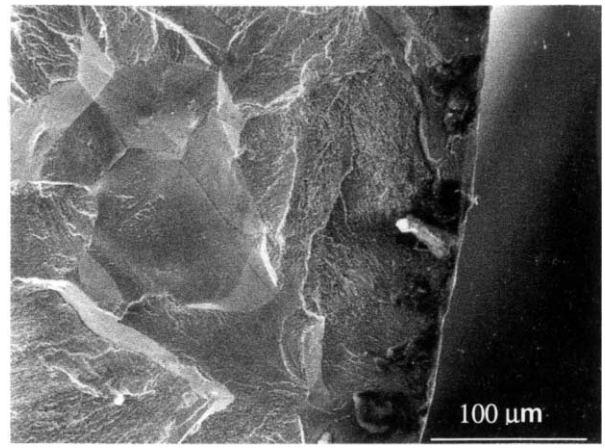


Fig. 11. SEM micrograph near the crack-initiation site of 316 LN SS (sample 5-E) tested at 10 Hz in mercury with $\sigma_{max} = 439$ MPa (247,648 cycles to failure).

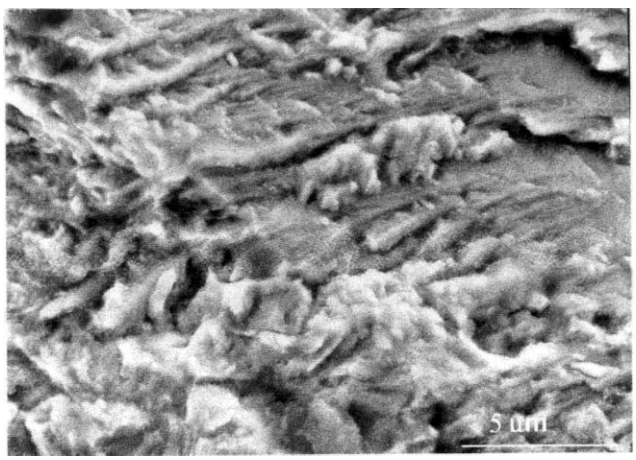


Fig. 9. SEM micrograph near the crack-initiation site of 316 LN SS (sample 1-A) tested at 10 Hz in air with $\sigma_{max} = 439$ MPa (341,408 cycles to failure).

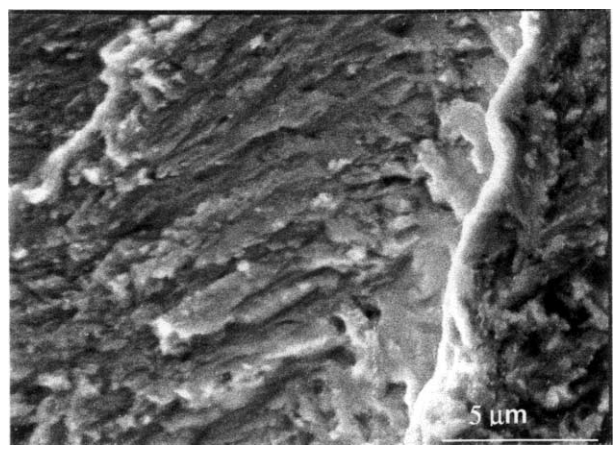


Fig. 12. SEM micrograph near the crack-initiation site of 316 LN SS (sample 5-E) tested at 10 Hz in mercury with $\sigma_{max} = 439$ MPa (247,648 cycles to failure).

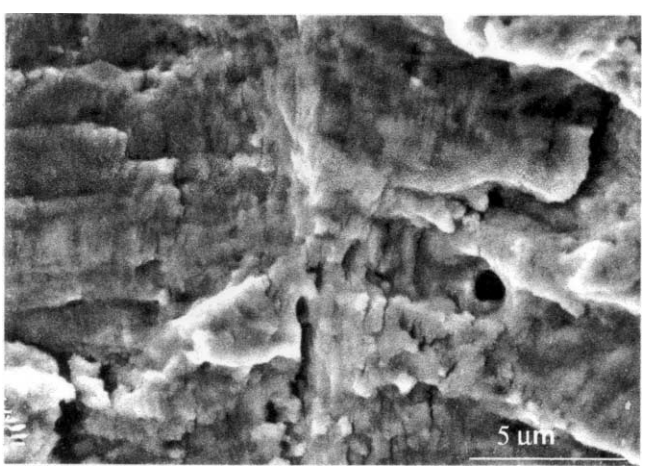


Fig. 10. SEM micrograph in the crack-propagation region of 316 LN SS (sample 1-A) tested at 10 Hz in air with $\sigma_{max} = 439$ MPa (341,408 cycles to failure).

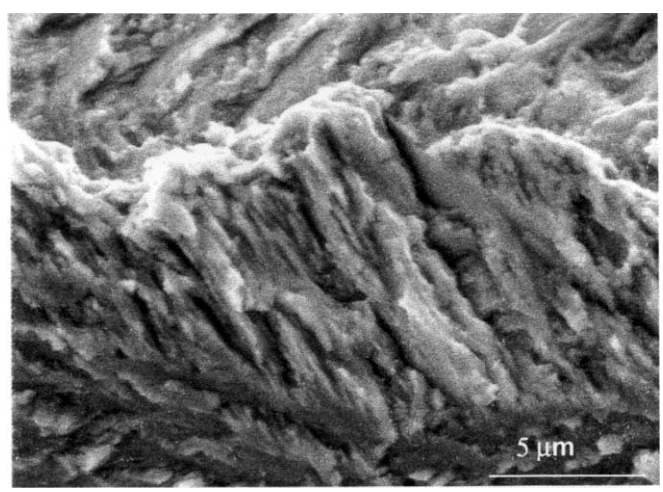


Fig. 13. SEM micrograph in the crack-propagation region of 316 LN SS (sample 5-E) tested at 10 Hz in mercury with $\sigma_{max} = 439$ MPa (247,648 cycles to failure).

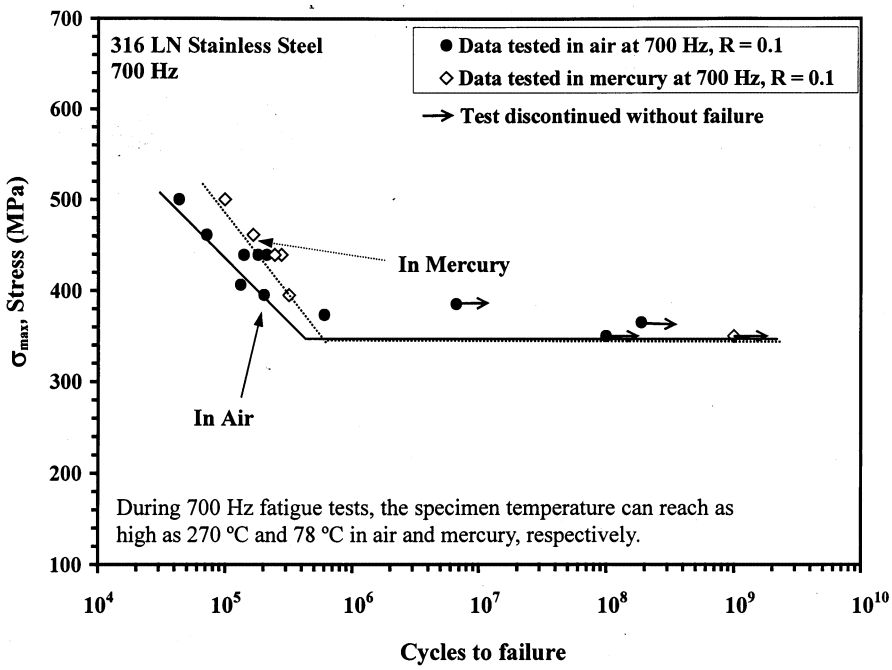


Fig. 14. Effect of test environment on the fatigue life of 316 LN SS at 700 Hz.

crease in sensitivity of the crack-initiation behavior to the specimen preparation and microstructure.

### 4.2. Test-frequency effect

As discussed previously, the target-container will be subjected to several types of loading conditions in its service environment. One of the loads on the target container is the thermal stress to the container, induced by direct heating from the proton beam. Another is the load transferred from the mercury pressure waves caused by beam pulses. As a result, the SNS target-container is subjected to fatigue loading at various frequencies. Thus, the influence of test frequency was investigated.

#### 4.2.1. Tests in air

Fig. 5 shows the results of HCF (high cycle fatigue) tests of 316 LN SS at the frequencies of 10 and 700 Hz. The fatigue life in air at the frequency of 700 Hz is shorter than that at 10 Hz, although the fatigue endurance limit tends to be comparable in both conditions. The difference in the fatigue lives at the two frequencies seems to increase with increasing maximum stress levels.

Further tests were performed concerning the temperature development in the 316 LN SS during HCF tests. The temperature variations during fatigue tests were determined using the IR camera, and they are illustrated in Fig. 6. Efforts were aimed at confirming the suggestion that an increase in the specimen temperature during a high-frequency test could be responsible for decreasing the fatigue life.

During fatigue testing, the temperature on the specimen gradually rose to reach a steady-state temperature after some time [21–23]. In the steady-state temperature range, the average temperature held constant for many cycles and occupied a significant portion of the fatigue life. The temperature was observed to oscillate with a small amplitude within each fatigue cycle. Before failure of the specimen, the temperature abruptly increased again, followed by a drop after the specimen failed. For the 700 Hz fatigue test of 316 LN SS with a maximum stress level of 439 MPa, the temperature increased to 270°C in the steady-state region.

During the initial period of fatigue, the temperature variation is due to thermoelastic and inelastic effects

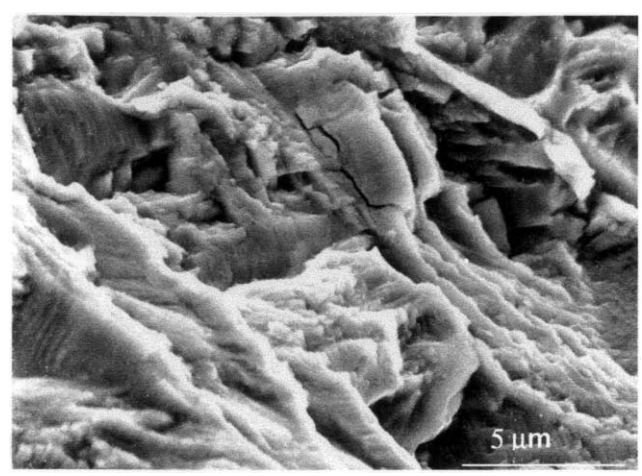


Fig. 15. SEM micrograph near the crack-initiation site of 316 LN SS (sample 4-D) tested at 700 Hz in air with $\sigma_{max} = 439$ MPa (181,774 cycles to failure).

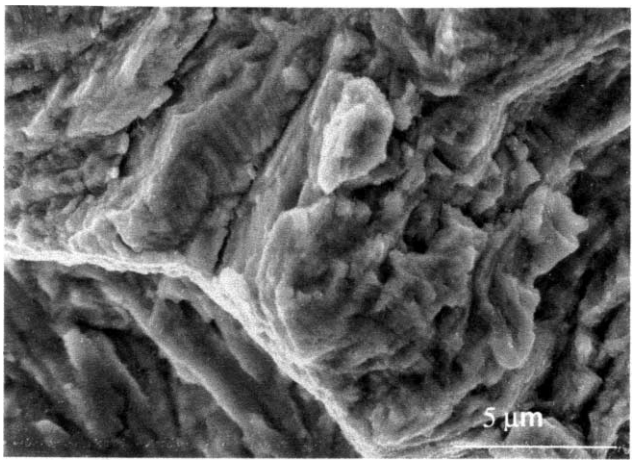


Fig. 16. SEM micrograph in the crack-propagation region of 316 LN SS (sample 4-D) tested at 700 Hz in air with $\sigma_{max} = 439$ MPa (181,774 cycles to failure).

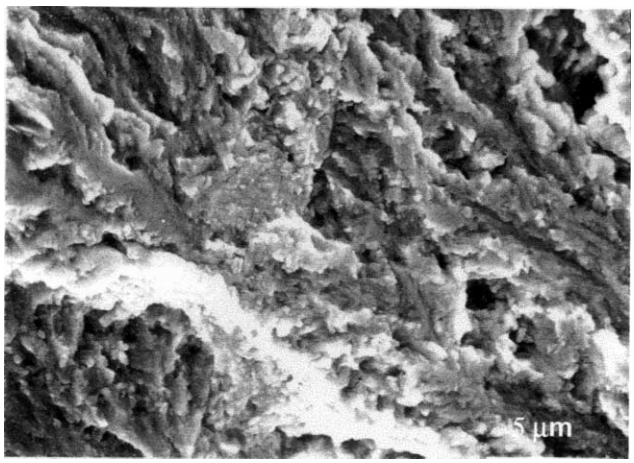


Fig. 17. SEM micrograph near the crack-initiation site of 316 LN SS (sample 6-F) tested at 700 Hz in mercury with $\sigma_{max} = 439$ MPa (276,750 cycles to failure).

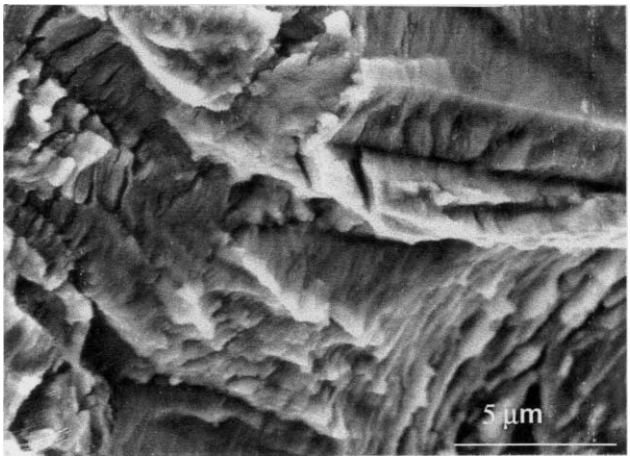


Fig. 18. SEM micrograph in the crack-propagation region of 316 LN SS (sample 6-F) tested at 700 Hz in mercury with $\sigma_{max} = 439$ MPa (276,750 cycles to failure).

[21–23]. The inelastic effects include plastic deformation and internal friction. The heat release speed is not as rapid as the heat accumlation, and therefore, the temperature increases. After a certain period of time, the buildup of temperature due to the internal friction and movement of dislocations (inelastic deformation) decreases as the material work hardens. At the higher temperature, the heat loss rate to the environments is also higher. Thus, the temperature of the material reaches a steady state. The final increase in temperature before failure of the specimen is related to the formation of cracks, which induces large plastic deformation and thus, an abrupt temperature rise [22,23]. Within each fatigue cycle, the temperature oscillation generally results from the thermoelastic effects.

In Fig. 6, the steady-state temperature measured by thermography is plotted as a function of the test frequency. At 10 Hz and $\sigma_{max} = 439$ MPa, the steady-state temperature is approx. 25°C in the air-environment fatigue test, which is much lower than that of 270°C at 700 Hz in the steady state. Correspondingly, the fatigue lives of 316 LN SS are longer at 10 Hz than at 700 Hz (Fig. 5).

The temperature difference gives a possible explanation for the effect of test frequency on fatigue lives in air. Since the steady-state temperature generally decreases with decreasing $\sigma_{max}$ [21–23], it is expected, and experimentally observed in Fig. 5, that the temperature difference between 10 and 700 Hz would decrease with decreasing $\sigma_{max}$.

#### 4.2.2. Tests in mercury

As shown in Fig. 7, the fatigue lives at 10 and 700 Hz in mercury appear to be similar in contrast with the results in air (Fig. 5), i.e., there is little influence of test frequency on the fatigue life in mercury. Note that the fatigue data at 10 Hz in mercury developed at UTK and ORNL are in good agreement, especially for the maximum stress levels above 420 MPa. However, at lower stress levels ($\leqslant 420$ MPa), some scatter of fatigue lives was observed.

In Fig. 6, the specimen temperature in the mercury-environment fatigue test at 700 Hz with the $\sigma_{max} = 439$ MPa was approx. 78°C, while at 10 Hz the temperature was approx. 25°C. The difference in specimen temperatures at these two frequencies in mercury is much smaller than the difference in air. Thus, the apparent frequency effect for the fatigue tests in mercury is not as significant as that in air.

### 4.3. Effect of environment

In the previous section, the test results were examined as a function of frequency in air and mercury. Here, the same results are examined at a fixed frequency.

#### 4.3.1. Tests at 10 Hz

Fatigue tests at the stress levels greater than 400 MPa in mercury at 10 Hz have shorter lives as compared with those in air (Fig. 8). However, for tests at lower stress levels ( $\leqslant$ 400 MPa), the material has comparable fatigue lives in mercury and air. For fatigue tests at higher stress levels (e.g. $>$400 MPa), LME is suggested to be the main factor that decreases the fatigue life of 316 LN SS. At higher stress levels, mercury may have more chance to interact directly with the fresh surface in the crack-tip area due to the larger plastic deformation. Thus, there is a greater possibility of better contact of the mercury with the fresh metal surface at higher stresses. Moreover, at high stress levels, the fatigue life is generally determined by the crack-propagation process. During the crack-growth period at high stress levels, the crack opening displacement (COD) is relatively large, which facilitates the penetration of mercury into the crack tip and the contact with the fresh crack surface. Correspondingly, the penetration depth of the mercury may be increased during a high-stress fatigue test, and wetting of the freshly cracked surface by mercury may be enhanced. These trends result in the mercury effects at high stress levels (Fig. 8).

The SEM micrographs of the fracture surfaces of the specimens tested at 10 Hz in air and mercury showed different fracture mechanisms. Figs. 9 and 10 are micrographs of the crack-initiation site and the crack-propagation region of 316 LN SS tested at 10 Hz in air, respectively. The specimen tested in air showed typical transgranular (TG) cracking throughout most of the fracture surface and a dimpled fracture in the overload region.

In contrast, the specimen tested in mercury exhibited intergranular (IG) cracking near the crack-initiation site, as shown in Fig. 11. Fig. 12 is the intermediate region showing where the cracking mode changed from IG to TG. In this region, the grain boundaries are already difficult to discern, and the broken surface exhibits a quasi-cleavage appearance. At the center part of the specimen, the fracture mechanism in the crack-growth region changed to a transgranular mode (Fig. 13). The intergranular-cracking region is believed to be a direct result of LME. But intergranular cracking seems not to be a widespread fracture mechanism for the 316 LN SS tested in mercury. This trend corresponds to the results reported by other authors [4–7].

At low stress levels ( $\leqslant$ 400 MPa), the fatigue lives in mercury are comparable with those in air at low stress levels as shown in Fig. 8. This trend can be explained as a result of lack of the penetration and wetting of mercury at low stresses.

#### 4.3.2. Tests at 700 Hz

Fig. 14 presents the $S$–$N$ curve for 700 Hz in air and mercury. Obviously, LME is not a factor in the fatigue behavior of 316 LN SS at 700 Hz in mercury. In fact, longer fatigue lives in mercury than in air were observed. Thermography tests showed that temperature might be the dominant factor that contributed to the difference in the fatigue life at 700 Hz in air and mercury. For the fatigue test at 700 Hz and $\sigma_{max} = 439$ MPa with a $R$ ratio of 0.1, the specimen temperature in air was much greater than that in mercury, approx. 270 versus 78°C (Fig. 6). Mercury serves as a heat sink and effectively lowers the specimen temperature at 700 Hz, which results in longer fatigue lives in mercury than air.

In Fig. 14, decreasing $\sigma_{max}$ decreases the difference in the fatigue lives in air and mercury. This trend can be expected to result from the fact that decreasing $\sigma_{max}$ reduces the specimen temperature in air [21–23].

The SEM micrographs of the specimens tested at 700 Hz in air and mercury are presented in Figs. 15–18. Whether at the crack-initiation site or in the crack-propagation region, any difference in cracking modes in air and mercury is difficult to distinguish. The initiation site showed similar TG features in air (Fig. 15) and mercury (Fig. 17). However, some striations, although difficult to resolve on the fracture surface of the specimens tested in air, indicate a greater extent of ductile fracture in air than mercury. The somewhat brittle appearance of cracking in mercury seems to suggest that LME may have occurred in specimens tested in mercury.

Table 3
Test-frequency and environmental effects on the fatigue behavior of 316 LN stainless steel

| Effects | | Fatigue behavior | |
|---|---|---|---|
| | | Phenomena | Mechanism |
| Test-frequency effect | Air | Significant shorter fatigue life at 700 than 10 Hz | Increase of the specimen temperature at a higher frequency |
| | Mercury | Insignificant difference in fatigue lives at 10 and 700 Hz | Mercury acting as a coolant, reducing the specimen temperature |
| Environmental effect | 10Hz | Shorter fatigue life in mercury at applied maximum stress levels $\geqslant$400 MPa than in air | Liquid-metal-embrittlement effect; better wetting between the mercury and steel at high stress levels |
| | 700 Hz | Longer fatigue life in mercury than in air | Insignificant LME effect; greater specimen temperature in air than in mercury |

Fig. 18 shows striations on the surface of specimens tested in mercury, which are not as clear as those in air (Fig. 16). Both fractographs (Figs. 16 and 18) exhibit typical TG cracking in the crack-propagation region, which means LME, if present, is not significant enough to result in an obvious difference in the fracture mode. The SEM micrograph of the specimens tested at 700 Hz in mercury did not show IG cracking (Figs. 17 and 18). However, there was TG cracking and some faint striations in Figs. 17 and 18, which were similar to those observed in the specimens tested in air (Figs. 15 and 16). This trend suggests that there is no significant LME in mercury at 700 Hz, because of the higher frequency and less time in each fatigue at 700 Hz, which decreases the mercury effect, relative to that at 10 Hz (Figs. 8 and 11).

## 5. Summary of test frequency and environmental effects

The present studies investigated two main factors that could have significant effects on the fatigue life of 316 LN SS in air and mercury: test frequency and environment. These two effects are summarized in Table 3 and in the discussion below.

### 5.1. Test frequency effect

The extent of the frequency effect on the fatigue life varies with the test environment. For the fatigue tests conducted in air, specimens generally have shorter fatigue lives at the high frequency of 700 Hz than those at the low frequency of 10 Hz. This trend is evidently the result of a greater increase in the specimen temperature at 700 Hz. Decreasing the applied maximum stress level decreases the frequency effect in air.

In contrast, for the mercury-environment fatigue tests, specimens show insignificant difference in the fatigue lives at 10 and 700 Hz. As the mercury acts as a heat sink, the difference in the specimen temperature induced at 10 and 700 Hz is not large enough to show an obvious frequency effect on the fatigue life.

### 5.2. Environmental effect

The environmental effect depends on both the stress level and test frequency. Fatigue tests conducted at the low frequency of 10 Hz have shorter fatigue lives at high maximum stress levels ($\geqslant 400$ MPa) in mercury, as compared to those in air. This trend is believed to result from LME in mercury. At lower applied stress levels, the fatigue lives in mercury and air are comparable.

For the fatigue tests carried out at the high frequency of 700 Hz, longer fatigue lives in mercury were observed, relative to those in air for the higher stress ($\geqslant 400$ MPa). However, decreasing the applied stress level at 700 Hz decreases the difference in the fatigue lives in air and mercury.

## 6. Conclusions

1. The specimen temperature developed during fatigue can greatly influence the effects of test frequency and environment on the fatigue life.
2. There is a frequency effect between 10 and 700 Hz in air. The greater specimen temperature at 700 than 10 Hz reduces the fatigue life at 700 Hz.
3. There is no significant frequency effect between 10 and 700 Hz in mercury.
4. Fatigue specimens tested at 10 Hz and applied maxmum stress levels over 400 MPa in mercury exhibit shorter lives, as compared to those in air, which may be due to liquid metal embrittlement.
5. Fatigue lives at 700 Hz in mercury were found to be generally longer than in air, resulting from a temperature effect due to the cooling effect of mercury compared with air.
6. The fatigue endurance limit measured at both 10 and 700 Hz in air and in mercury was approx. 350 MPa.

## Acknowledgements

This research was sponsored by the Division of Materials Sciences, US Department of Energy under contract DE-AC05-96OR22464 with the Lockheed Martin Energy Research Corporation. The authors acknowledge J.T. Broome, L. Jiang, B. Yang, Drs. C.R. Brooks, K. Farrell, S.J. Pawel, G.T. Yahr, L. Chen, and Y. He for their careful instructions and helpful suggestions on the fatigue tests. We also acknowledge the financial support of the National Science Foundation, the Division of Design, Manufacture, and Industrial Innovation, under Grant No. DMI-9724476, the Combined Research-Curriculum Development (CRCD) Program, under EEC-9527527, and the Integrative Graduate Education and Research Training (IGERT) Program, DGE-9987548, to the University of Tennessee, Knoxville, with Dr D.R. Durham, Ms M. Poats, and Dr W. Jennings as program managers, respectively. We appreciate the financial support of the Center for Materials Processing and Office of Research Administration at the University of Tennessee, Knoxville.

## References

[1] L.K. Mansur, H. Ullmaier, Proceedings of the International Workshop on Spallation Materials Technology, Oak Ridge Na-

tional Laboratory Report CONF-9604151, Oak Ridge, TN, 23 April, 1996.
[2] T.A. Gabriel, J.M. Barnes, L.A. Charlton, J. DiStefano, K. Farrell, J. Haines, et al., Proceedings of the Topical Meeting on Nuclear Applications of Accelerator Technology, Albuquerque, NM, 6 November, 1997, American Nuclear Society, pp. 288–292.
[3] W. Rostoker, J.M. McCaughey, H. Markus, Embrittlement by Liquid Metals, Reinhold, New York, 1960.
[4] J.J. Krupowicz, Journal of Engineering Materials and Technology 111 (1989) 229.
[5] C.E. Price, L.B. Traylor, National Association of Corrosion Engineers 43 (1987) 229.
[6] C.E. Price, J.K. Good, Transactions of the ASME 106 (1984) 178.
[7] C.E. Price, R.G. Norman, Acta Metallurgica 35 (1987) 1639.
[8] D.A. Wheeler, R.G. Hoagland, J.P. Hirth, Corrosion 45 (1989) 207.
[9] J.A. Kapp, D. Duquette, M.H. Kamdar, Journal of Engineering Materials and Technology 108 (1986) 37.
[10] L.A. Charlton, L.K. Mansur, M.H. Barnett, R.K. Corzine, D.J. Dudziak, M.S. Wechsler, Second International Topical Meeting on Nuclear Applications of Accelerator Technology, Gatlinburg, TN, 20 September, 1998, American Nuclear Society, pp. 247–253.
[11] M.S. Wechsler, M.H. Barnett, D.J. Dudziak, R.K. Corzine, Proceedings of the Topical Meeting on Nuclear Applications of Accelerator Technology, Albuquerque, NM, 16 November, 1997, American Nuclear Society, pp. 21–28.
[12] S.J. Pawel, J.R. DiStefano, E.T. Manneschmidt, Oak Ridge National Laboratory Report ORNL/TM-13754, April 1999.
[13] L.K. Mansur, J.R. Distefano, K. Farrell, E.H. Lee, S.J. Pawel, M.S. Wechsler, Proceedings of the Topical Meeting on Nuclear Applications of Accelerator Technology, Albuquerque, NM, 16 November, 1997, American Nuclear Society, pp. 301–311.
[14] R.W. Swindeman, ORNL/NPR-92/24, June 1993.
[15] K.M. Nikbin, G.A. Webster, N. Mitchell, Fusion-Engineering-and-Design 29 (1995) 421.
[16] A. Nyilas, H. Yanagi, Cryogenics 29 (1989) 191.
[17] X. Sun, J. Xu, Y. Li, Materials Science Engineering A114 (1989) 179.
[18] M.P. Mishra, C.C. Packiaraj, S.K. Ray, S.L. Mannan, H.U. Borgstedt, International Journal of Pressure Vessels and Piping 70 (1997) 77.
[19] R.S. Dutta, P.K. De, H.S. Gadiyar, Corrosion Science 34 (1993) 51.
[20] S.J. Pawel, J.R. DiStefano, L.K. Mansur, K. Farrell, J.P. Strizak, T.S. Byun, Proceedings of the Third International Topical Meeting on Nuclear Applications of Accelerator Technology, Long Beach, CA, 14 November, 1999, American Nuclear Society, pp. 117–128.
[21] P.K. Liaw, H. Wang, L. Jiang, B. Yang, J.Y. Huang, R.C. Kuo, et al., Scripta Materia 42 (2000) 389.
[22] H. Wang, L. Jiang, P.K. Liaw, D.L. Klarstrom, Metallurgical and Materials Transactions A 31 (2000) 1307.
[23] B. Yang, P.K. Liaw, H. Wang, L. Liang, J.Y. Huang, R.C. Kuo, et al., Mater. Sci. Eng. A 314 (2001) 133–141.